Spectral and Temporal Properties of Optical Signals with Multiple Sinusoidal Phase Modulations

Introduction

High-energy laser systems have been developed for exploring regimes of high-intensity interaction of light with matter, e.g., plasma physics, astrophysics, and the generation of particles. One application of these lasers is inertial confinement fusion (ICF)—a strategy for producing energy by compressing and heating capsules filled with hydrogen isotopes and igniting fusion reactions that release a large number of energetic neutrons.[1,2] Laser systems developed for ICF are large-scale complex optical systems that must produce temporally shaped optical pulses containing megajoules of energy in the ultraviolet (UV).[3,4] The laser–target interaction is an intensity-dependent process that requires the time-dependent power of the optical pulses to be precisely shaped. Temporal phase modulation must be added to prevent damage to the laser system and smooth out intensity variations at the surface of the target. High-intensity narrowband optical waves lead to stimulated Brillouin scattering (SBS) in optical components with potentially catastrophic consequences.[5] The growth of SBS waves is inhibited by increasing the bandwidth of the optical wave, typically by phase modulation in the low-energy front end to generate multiple sidebands. Phase modulation at a few GHz's with index modulation sufficient to create approximately ten sidebands is used on systems like the National Ignition Facility (NIF) and the Laser Mégajoule Facility (LMJ).[5–7] Uniform compression of the target is required to reach the conditions for fusion in the target core, but such compression is hindered by instabilities.[8] Smoothing by spectral dispersion (SSD) reduces the fluence variations of individual beams to produce a target irradiation that is spatially uniform on a time-averaged basis.[9–11] SSD uses temporal phase modulation to induce a time-dependent instantaneous frequency on the optical pulse. A phase plate placed before the focusing component at the end of the laser system creates a highly modulated far field composed of speckles.[12] A diffractive component in the laser system ensures that the far-field position depends on the optical frequency. The combination of time-varying instantaneous frequency, frequency-dependent far-field position, and highly modulated far field is used to obtain a uniform target illumination when averaged over the duration of the optical pulse. The NIF and the LMJ were built for indirect drive—an approach to ICF where the target is compressed by x rays generated when the optical pulses interact with the walls of a hohlraum.[1] In this approach, phase modulation at a single frequency with a modulation index of a few radians is sufficient for SSD when implemented with angular dispersion in only one direction. In the direct-drive approach to ICF, the optical pulses directly compress the target.[2] If SSD is implemented in only one direction, modulation at multiple frequencies is required, at least during the low-energy portion of the pulse shape.[11,13] Theoretical studies and experimental demonstration of a system combining pulses with three high-frequency phase modulations and pulses with SBSS (SBS suppression) and single-frequency SSD have been performed.[14–16] Optical pulses with multiple temporal phase modulations are routinely used on these high-energy laser facilities for reducing the threat of SBS and optimizing the target illumination by SSD.

A known issue when using phase-modulated optical pulses is the conversion of frequency modulation to amplitude modulation (FM-to-AM conversion).[7,17–19] A pulse of constant power with a single sinusoidal temporal phase modulation at frequency f has spectral sidebands at frequencies separated by f with spectral density given by Bessel functions of the first kind and precise phase relations.[20] When the spectral amplitude and/or phase of these sidebands are modified, the power becomes time dependent, e.g., it has a sinusoidal modulation at frequency f. A modification of the time-varying power of the shaped pulse might be detrimental to the interaction of the pulse with the target. It can also lead to optical damage in the laser system by increasing the peak power beyond the damage threshold of optical components. Sources of FM-to-AM conversion include chromatic dispersion, wavelength-dependent gain of laser amplifiers, generation of low-energy replicas interfering with the main signal, and spectral clipping. Studies of FM-to-AM conversion in pulses with a single phase modulation are available in the literature. Examples of FM-to-AM conversion of signals with SBSS at 2 GHz and SSD at 14.25 GHz have been presented in the context of the LMJ,[7] but no general study for pulses with multiple phase modulation (multi-FM) has been published. This study is highly relevant to the operation of cur-

rent systems and engineering of future systems because these systems typically use phase modulation at multiple frequencies.

This article first presents a statistical study of the optical spectrum of multi-FM signals. The optical spectrum of these signals is shown to converge to a normal distribution using an analogy with the statistical properties of the probability density function of the sum of independently distributed variables, which allows one to use the central limit theorem. Convergence of the frequency integral of the spectral density to the cumulative density function of the normal distribution makes it possible to predict the frequency range containing a given fraction of the total energy. The statistical study is followed by general derivations of FM-to-AM conversion in optical signals with multiple phase modulations from linear and quadratic spectral amplitude modulation, for example, resulting from spectral filters and optical amplifiers and from quadratic and cubic spectral phase modulations, for example, caused by chromatic dispersion in optical fibers in the front end. These impairments are inherently present in high-energy laser systems because of their architecture and component availability. Compensation subsystems must be developed so that the transfer function of the entire laser system does not lead to FM-to-AM conversion. These compensators are, for example, Lyot-type filters that compensate for the gain narrowing in a Nd:glass amplifier and a grating compressor that compensates for chromatic dispersion.[6,16] The design and performance of these subsystems are intrinsically linked to understanding the modulation magnitude in critical parts of the system where optical damage might occur. FM-to-AM conversion caused by the nonlinear frequency conversion from the infrared to the ultraviolet is not treated but could be the subject of further studies based on what is already known for single-frequency modulation.[7,18,19,21] FM-to-AM conversion from free-space propagation close to image planes of the diffraction grating used for SSD is described by a quadratic spectral phase[7,14] and can be treated with the same formalism. Another source of FM-to-AM conversion in high-energy laser systems is the interference of multiple replicas of the main pulse generated during amplification in the fiber front end.[17,22] This is inherent to the propagation of polarized signals in polarization-maintaining optical fibers having a finite extinction ratio, but the associated AM can be significantly reduced via engineering, in particular using optical fibers that transmit light along only one well-defined polarization[17] or alternating the orientation of the fast and slow axes of the optical fibers.[22]

For the impairments considered in this article, the amplitude modulation is evaluated by two metrics without frequency resolution: peak-to-valley (PV) and root-mean-square (rms) modulation on the temporal pulse, and by the PV modulation at specific frequencies. The specific frequencies are the individual modulation frequencies f_n in the case of linear amplitude modulation and quadratic phase modulation. They are the sums and differences of modulation frequencies $f_i \pm f_j$ for quadratic amplitude modulation and cubic phase modulation. Evaluating the amplitude modulation on the temporal pulse is crucial to setting allowable limits for individual impairments. Evaluating the modulation at specific frequencies helps to interpret time-resolved measurements provided by high-bandwidth diagnostics. Bandwidth-limited measurements of the instantaneous power can be interpolated at high frequencies not measured by the diagnostic. It is conceivable that limiting impairments can be identified from the spectral signature of the measured relative modulations at different frequencies.

The following sections (1) present general notations and definitions; (2) present a statistical approach to predicting the spectrum of signals with multiple sinusoidal phase modulations and frequency intervals containing a given fraction of the total energy; (3) describe FM-to-AM conversion in the presence of linear amplitude modulation and quadratic phase modulation, which leads to amplitude modulation at the phase-modulation frequencies; (4) detail FM-to-AM conversion in the presence of quadratic amplitude modulation and cubic phase modulation, which leads to amplitude modulation at combinations of the phase-modulation frequencies; and (5) present additional considerations and conclusions.

General Considerations

1. Definitions

An initially monochromatic field at the frequency ω_0 is modulated at multiple microwave frequencies $f_j = \Omega_j / 2\pi$ with respective modulation index m_j. For simplification, the oscillating term resulting from ω_0, present in all the temporal fields, is not written, and spectral fields are consistently plotted after translation by ω_0; i.e., with a zero carrier frequency. The phase modulations are co-phased at $t = 0$ for the derivation of FM-to-AM conversion. One reason for doing so is that for a small number of modulation frequencies, one can identify a time around which the sinusoidal modulations are co-phased, i.e., reach a maximum. This is justified by the absence of correlation for the values of sinusoidal modulations at non-commensurate frequencies. As such, the probability that one reaches a maximum around a given time is uncorrelated to the probability that the others reach a maximum around the same time, and the probability that they are all within some range of their maximal value at a given time is the product of the

individual probability, which is nonzero. Various simulations with co-phasing and with random relative phases on monochromatic fields have led to similar results, and the relative phase of the uncorrelated sinusoidal modulations generally does not play a significant role when calculating the overall amplitude modulation in a PV and rms sense. When using a pulse of finite duration, the relative phases of the temporal phase modulations and their timing relative to the power of the pulse play a role, e.g., the maximum PV modulation might not be reached over the finite time interval where the pulse power is nonzero. The derivations presented here correspond to a worst-case scenario, where the amplitude modulations are considered over a very large temporal range. With these conventions, the temporal field is simply written as

$$E(t) = \exp\left[i \sum_j m_j \cos\left(\Omega_j t\right)\right]. \tag{1}$$

2. Parameters for Derivations and Simulations

The analytical derivations are performed for an arbitrary number of noncommensurate microwave frequencies of arbitrary modulation index with impairments leading to a small change in the electric field of the optical pulse, i.e., inducing a small amplitude modulation. This is the useful range for application to high-energy lasers since the impairments and amplitude modulation must be minimized. Signals with commensurate frequencies have been studied in the context of providing a uniform spectral density over a given bandwidth, but the resulting on-target smoothing might be impacted by resonances.[23] These signals should be the subject of a separate study if they find an application for beam smoothing. Simulations have been performed with the parameters defined in Ref. 16 for the so-called picket channel. The corresponding frequencies and modulation indices are given in Table 136.III and a detail of the phase modulations is shown in Fig. 136.19(a). The optical signal obtained by phase modulation with these parameters is called the "test signal" for the remainder of this

article. These parameters were determined by simulations to optimize the on-target smoothing, including the engineering constraints related to potential implementation on the NIF.[13] Small relative changes to these frequencies would not affect the smoothing, but they have been chosen as multiples of a reference clock available at the Omega Laser Facility because this allows them to be temporally synchronized to the optical pulse. The microwave frequencies are commensurate, but the integer multiples linking them are so large that no effect of commensurability has been observed in simulations. The resulting optical spectrum is shown in Fig. 136.19(b). A Gaussian spectral density with an identical rms bandwidth (50 GHz) has been plotted, as discussed in the next section.
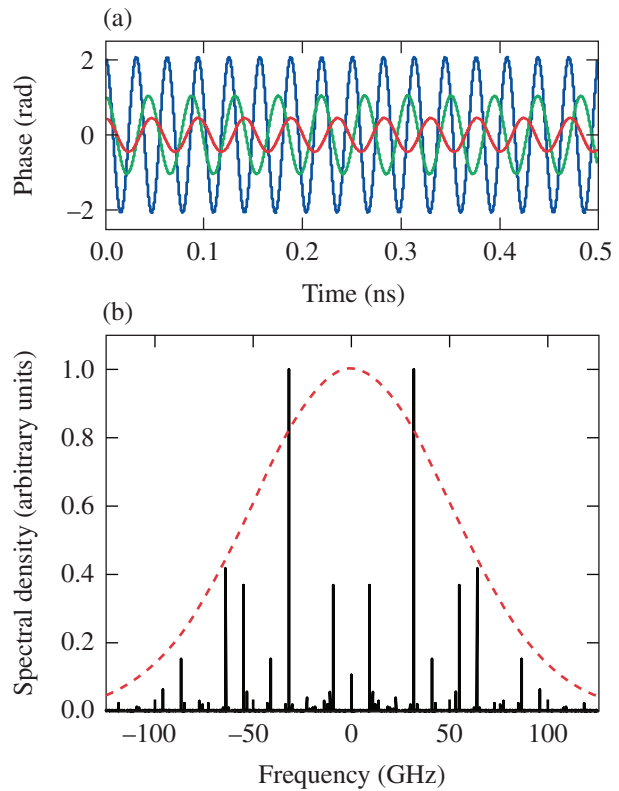
E22665JR

Figure 136.19
(a) Phase modulations used for simulations with parameters given in Table 136.III (f_1, f_2, and f_3 plotted in red, green, and blue, respectively). (b) Optical spectrum resulting from these phase modulations applied to a monochromatic field (black solid line) and Gaussian spectrum with identical root mean square (rms) bandwidth (red dashed line).

The considered spectral impairments are linear amplitude modulation (parameter l), quadratic amplitude modulation (parameter q), quadratic phase modulation (parameter φ_2), and cubic phase modulation (parameter φ_3), with transfer function given, respectively, by

Table 136.III: Characteristics of the phase modulations used for simulations. All frequencies are multiples of the reference frequency f_{ref} = 37.998935 MHz.

Modulation	Frequency (GHz)	Multiple of f_{ref}	Modulation index (rad)
Multi-FM-1	$f_1 = 21.165$	557	0.45
Multi-FM-2	$f_2 = 22.837$	601	1.04
Multi-FM-3	$f_3 = 31.881$	839	2.07

$$\tau(\omega) = \sqrt{1 + l\omega}, \tag{2}$$

$$\tau(\omega) = \sqrt{1 + q\omega^2}, \tag{3}$$

$$\tau(\omega) = \exp\left(i\varphi_2\omega^2 / 2\right), \tag{4}$$

$$\tau(\omega) = \exp\left(i\varphi_3\omega^3 / 6\right). \tag{5}$$

The range of impairment parameters for simulations was arbitrarily chosen between 0 and a maximal value calculated so that for amplitude impairments, the magnitude of the transfer function reaches the value 1.2 at $f = 100$ GHz and for phase impairments, the phase of the transfer function reaches the value 0.2 rad at $f = 100$ GHz. The parameters l, q, φ_2, and φ_3 are chosen positive to simplify the equations.

**Spectrum and Bandwidth of Signals
with Multiple Phase Modulations**
1. Spectrum and Bandwidth of Signal
   with Single Phase Modulation
   Signals with a single temporal phase modulation are widely used in telecommunications and their spectral properties are well documented.[20] The optical spectrum of a signal with phase modulation at frequency Ω with index m is composed of discrete sidebands at the frequencies $n\Omega$ and power given by the Bessel function of the first kind $\left| J_n(m) \right|^2$. According to Carson's rule, 98% of the energy is contained in the bandwidth

$$\mathrm{BW}_{98\%} = 2(m+1)\Omega. \tag{6}$$

Knowledge of the spectral properties of signals with multiple phase modulations can be obtained using statistical arguments, as shown in this section. One approach for obtaining an operational definition of the bandwidth of these signals is to use the bandwidth of the spectrum $S(\omega, m, \Omega) = \left| \tilde{E}(\omega, m, \Omega) \right|^2$ in the rms sense,

$$\mathrm{BW}_{\mathrm{rms}}(m,\Omega) = \sqrt{\int \omega^2 S(\omega,m,\Omega)\,\mathrm{d}\omega \Big/ \int S(\omega,m,\Omega)\,\mathrm{d}\omega}, \tag{7}$$

which can be expressed using the properties of the Fourier transform as

$$\mathrm{BW}_{\mathrm{rms}}(m,\Omega) = \sqrt{\int \left| \frac{\partial E}{\partial t}(t) \right|^2 \mathrm{d}t \Big/ \int \left| E(t) \right|^2 \mathrm{d}t}. \tag{8}$$

Equation (8) is straightforward to calculate, resulting in

$$\mathrm{BW}_{\mathrm{rms}}(m,\Omega) = m\Omega / \sqrt{2}. \tag{9}$$

2. Bandwidth of Signals with Multiple Phase Modulations
   Equation (8) can be extended to a signal with multiple phase modulations given by Eq. (1):

$$\mathrm{BW}_{\mathrm{rms}}\left(\{m_j,\Omega_j\}\right) = \sqrt{\int \left[\sum_j m_j \Omega_j \sin(\Omega_j t) \right]^2 \mathrm{d}t}, \tag{10}$$

where the square can be expanded to give

$$\mathrm{BW}_{\mathrm{rms}}\left(\{m_j,\Omega_j\}\right) =$$
$$\sqrt{\sum_{j,k} m_j m_k \Omega_j \Omega_k \int \sin(\Omega_j t) \sin(\Omega_k t)\,\mathrm{d}t}. \tag{11}$$

For noncommensurate frequencies (Ω_j, Ω_k), the integral in Eq. (11) is 0, while for $j = k$, the integral is equal to 1/2, leading to the expression

$$\mathrm{BW}_{\mathrm{rms}}\left(\{m_j,\Omega_j\}\right) = \sqrt{\sum_j m_j^2 \Omega_j^2 / 2}. \tag{12}$$

The rms bandwidth of a signal with multiple noncommensurate phase modulations is the root mean square of the individual rms bandwidths.

An alternate way to obtain this result is to consider that the temporal electric field of a signal with multiple phase modulations is the product of the fields corresponding to individual phase modulations. In the spectral domain, this implies that the resulting field is the convolution of the individual fields. Because the modulation frequencies are not commensurate, the optical frequency of each sideband in the resulting spectrum is obtained by a unique linear combination of the optical frequencies of the sidebands of the individual fields. The amplitude of that sideband in the convolved field is given by a product of the amplitudes in each individual field. As a result, the power of that sideband is given by a product of the corresponding powers. The optical spectrum of the signal with multiple phase modulations is the convolution of the spectra corresponding to the individual modulations only when the modulation frequencies are non-commensurate. This general result was used in Ref. 7 for the two particular frequencies corresponding to SBSS and

SSD on the LMJ. From the general properties of the Fourier transform, it is known that the rms width of a convolution of multiple functions is equal to the rms of the individual rms widths, which confirms Eq. (12).

3. Spectrum of Signals with Multiple Phase Modulations

Obtaining an approximation of the spectrum of a signal with multiple phase modulations is important to quantify the energy present in a particular frequency interval. A comparison of Eqs. (6) and (9) indicates that the rms width and the Carson's rule bandwidth are loosely connected for arbitrary values of the modulation index. The rms width is computationally easy to use but it is not a precise indicator of the energy fraction present in a given frequency interval. One possible strategy to obtain useful information about the spectral density of a signal given by Eq. (1) is to formally reconsider the property that the resulting spectrum is the convolution of the individual spectra for modulation parameters (m_j, Ω_j) in light of the probability theory.

One considers N independent random variables $\{\omega_j\}$, where each random variable ω_j has a probability density function (pdf) given by $S(\omega, m_j, \Omega_j)$. Since the modulation frequencies are different, the probability density functions are different and the variables are not identically distributed. The convolution of these spectra, $S(\omega, \{m_j, \Omega_j\})$ is the pdf of the sum of the N random variables

$$S_N = \sum_j \omega_j$$

because of the probabilistic independence. The sum of a large number of independent and identically distributed variables with zero mean is probabilistically described by the central limit theorem, which states that the probability density function of the sum converges to a normal distribution with variance equal to N times the individual variance. This result is true in some conditions for the sum of N random variables that are independent but not identically distributed: the probability density function of the sum also converges to a normal distribution with variance given by the sum of the individual variances.[24] The sum cumulative distribution function (cdf) converges to the cdf of that normal distribution. A sufficient condition for convergence is that the third-order moment of the absolute value of each individual variable is finite. It is straightforward to simulate this quantity for Bessel spectra and conclude that this is the case. This makes it possible to conclude that the spectrum of the field given by Eq. (1) converges to a Gaussian function with standard deviation given by Eq. (12) for a large

number of modulation frequencies. The normal distribution and its cdf are well documented. For a normally distributed random variable x with unity standard deviation, the probit function, i.e., the quantile function (inverse of the cdf) of the normal distribution, yields the quantity x_p, defining the interval $]-\infty, x_p]$, corresponding to a statistical probability p (Ref. 25). For a Gaussian spectral density of standard deviation σ, the probit function gives the multiple x_p, defining the interval $]-\infty, \sigma x_p]$, containing the fraction p of the signal energy. Symmetric intervals $[-f_p, f_p]$ containing 98% of the energy, are considered in this article to be consistent with Carson's rule for a single modulation frequency. Considering the symmetry of the normal distribution, the frequency f_p is the product of the standard deviation by the probit function applied to $p = 0.99$, i.e., $f_p = 2.326\,\sigma$.

4. Simulations

The optical spectrum of signals with multiple phase modulations has been simulated for a variety of situations. The cumulative distribution function for the test-signal spectrum shown in Fig. 136.19(b) is displayed in Fig. 136.20. The cdf of a normal distribution with identical rms bandwidth (50 GHz) is also plotted for comparison. The agreement between these two curves is good. The cdf calculated from the spectrum reaches 99% at ~99 GHz, indicating that 98% of the energy is contained in the frequency interval 2×99 GHz = 198 GHz (note that the cdf is by definition an integral starting at $-\infty$, while the bandwidth of interest is defined as a symmetric interval centered at the
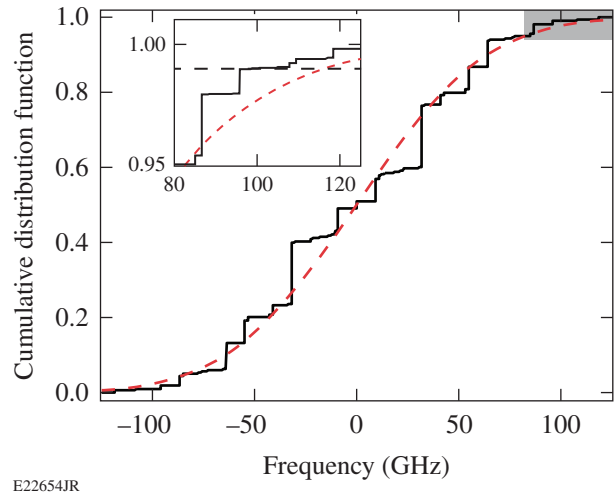

E22654JR

Figure 136.20
Cumulative density function of the spectrum shown in Fig. 136.19(b) (black solid line) and the Gaussian function with identical rms bandwidth (red dashed line). The inset is a close-up of the tail of the cumulative density functions at high frequencies, where a horizontal dashed line has been added to show the frequency values at which the two functions reach 0.99.

zero frequency). The 98% bandwidth of the Gaussian spectral density with rms bandwidth equal to 50 GHz is $2 \times 2.326 \times 50$ GHz = 233 GHz. The ratio of the actual 98% bandwidth to the 98% bandwidth predicted by the normal distribution is $\rho = 0.85$. The inset in Fig. 136.20 displays a close-up of the two cumulative density functions at high frequencies, confirming the discrepancy for the predicted 98% bandwidth. It is clear from this inset that the spectrum of the test signal is more concentrated and expands less toward high frequencies. The 17% overestimate predicted by the normal distribution is consistent with the more-general results obtained below.

Statistical simulations were performed to quantify the convergence of the spectrum of a multi-FM signal to its Gaussian approximation and of the corresponding cdf's. Figure 136.21 shows simulation results for the ratio ρ of the bandwidth containing 98% of the energy calculated from the spectral density to the bandwidth containing 98% of the energy assuming that the spectrum is Gaussian with standard deviation given by Eq. (12). For each number of modulation frequencies N (horizontal axis, from 1 to 10 on the left plots and 10 to 100 on the right plots) the standard deviation of the modulation index σ_m was allowed to vary between 1 and 5 (vertical axis). For each combination of N and σ_m, 1000 random draws of the modulation indices and modulation frequencies were made. For each draw, the modulation index is normally distributed with standard deviation σ_m and the modulation frequencies are initially normally distributed with standard deviation equal to 1 but are rescaled so that the rms bandwidth of the resulting signal is 100 GHz, following Eq. (12). This rescaling allows one to standardize the simulation results and necessary sampling in the time and frequency domain. Because it would be, in practice, difficult to co-phase a large number of sinusoidal modulations, the relative phase of the N modulations was chosen as a random variable uniformly distributed between 0 and 2π. This procedure allows one to map a wide range of multi-FM signals. The results displayed in the first row of Fig. 136.21 are the average values of the ratio ρ as a function of σ_m and N. For example, $\langle \rho \rangle = 1$ means that the 98% bandwidth of the calculated spectrum and Gaussian approximation are on average the same; values lower than 1 indicate that the Gaussian function overestimates the 98% bandwidth. The second row of Fig. 136.21 represents the standard deviation of the ratio ρ calculated over the 1000 random draws performed for the N modulation frequencies and modulation indices of standard deviation σ_m.

The optical spectrum of the phase-modulated fields effectively converged to a Gaussian distribution, and the cumulative
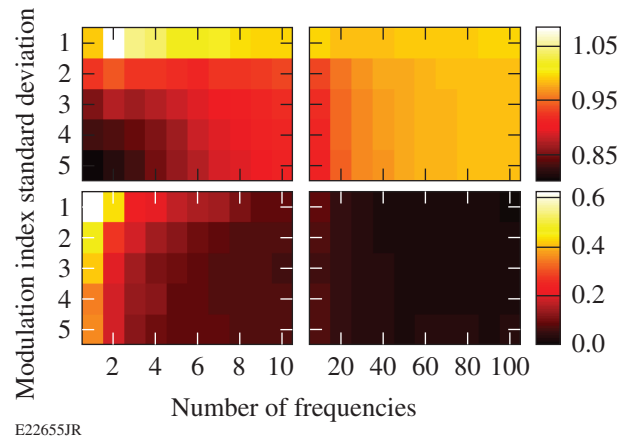

Figure 136.21
Statistics for the ratio ρ of the bandwidths containing 98% of the energy calculated from the spectral density of a multi-FM spectrum and directly calculated from the modulation parameters (frequencies and indices) assuming a normal spectral density. The upper and lower rows correspond to the average value and standard deviation, respectively, determined as a function of the number of modulation frequencies and standard deviation of the modulation index. The statistics are calculated over 1000 random draws of the modulation parameters.

distribution function of the spectrum converged to the corresponding cdf as the number of frequencies was increased. A strong correlation between the convergence of the cdf and the convergence of $\langle \rho \rangle$ toward 1 was observed, making it possible to discuss the following general spectral properties in light of the bandwidth results presented in Fig. 136.21:

- The spectrum approximation by a normal distribution gets better as the number of modulation frequencies increases. The average value of the ratio ρ converges to 1 and the standard deviation around the average value decreases as N increases. This is expected because the central limit theorem applies to the sum of a large number of independent variables.

- The ratio ρ is in most cases smaller than 1, meaning that the calculated spectrum is more concentrated toward lower frequencies than its normal approximation. This can be explained by the squarish shape of the spectrum of phase-modulated signals, which leads to more energy concentration for a given standard deviation. Predicting the spectral extent of a multi-FM signal using its rms bandwidth and the normal approximation leads to an overestimate.

- Small phase-modulation indices lead to a better approximation than large modulation indices; in particular for $\sigma_m = 1$, the normal approximation is good in an average sense even

for a small number of modulation frequencies. This is caused by the general shape of the spectrum of sinusoidally modulated signals: for a single phase modulation with low modulation index, the spectrum is close to a bell-shaped curve multiplied by a frequency comb at the modulation frequencies. Since the individual probability density functions are closer to normal distribution, the convergence of the probability density function of the sum of the variables to a normal distribution is faster.

- The spread of the simulated ρ relative to the average value is smaller as the number of frequencies increases (consequence of the central limit theorem) and as the modulation index increases for a given number of frequencies. The latter is attributed to the larger number of spectral modes resulting from larger modulation indices, leading to a smoother cdf because the spectral density of individual modes is on average smaller.

Impairments Leading to FM-to-AM Conversion at the Modulation Frequencies

1. Linear Spectral Amplitude

A linear spectral modulation corresponds, for example, to amplification at a frequency detuned from the maximum of an amplifier gain. The corresponding transfer function over the bandwidth of the pulse is

$$\tau(\omega) = \sqrt{1 + l\omega} \approx 1 + \frac{l}{2}\omega. \tag{13}$$

The temporal field after this transfer function is

$$E' = E + \frac{il}{2}\frac{\partial E}{\partial t}. \tag{14}$$

With the expression of the initial electric field given by Eq. (1), the modulated field is

$$E'(t) = E(t)\left[1 + \frac{l}{2}\sum_j m_j\,\Omega_j \sin\left(\Omega_j t\right)\right], \tag{15}$$

and the modulated power at first order in l is

$$P'(t) = 1 + l\sum_j m_j\,\Omega_j \sin\left(\Omega_j t\right). \tag{16}$$

Equation (16) shows that the modulation on the output pulse is at the modulation frequencies Ω_j with PV amplitude

$$\mathrm{PV}\left(\Omega_j\right) = 2lm_j\,\Omega_j. \tag{17}$$

The highest modulation is observed at the frequency for which the associated bandwidth $m_j\Omega_j$ is maximal. With noncommensurate modulation frequencies, there are times when the modulations in Eq. (16) are simultaneously close to a maximum and other times at which they are simultaneously close to a minimum. The PV modulation is given by

$$\mathrm{PV} = 2l\sum_j m_j\,\Omega_j, \tag{18}$$

and the rms modulation for these uncorrelated sinusoidal modulations is given by

$$\mathrm{rms} = l\sqrt{\sum_j m_j^2\,\Omega_j^2\big/2}. \tag{19}$$

Simulation results for the test signal are shown in Figs. 136.22 and 136.23. Figure 136.22 displays the modulated temporal power corresponding to a linear spectral amplitude modulation $l = 0.44/(100\ \mathrm{GHz})$: it is dominated by the modulation at the highest frequency f_3 but the influence of other frequencies can be seen as the slight modulation of the local power extrema. Figure 136.23 compares simulated and analytical results for the modulations determined without frequency resolution (PV and rms AM) [Eqs. (18) and (19)] and at the three modulation frequencies [Eq. (17)]. An excellent agreement is obtained. The highest modulation is observed at the frequency f_3 since that frequency corresponds to the highest product $m_j\Omega_j$.
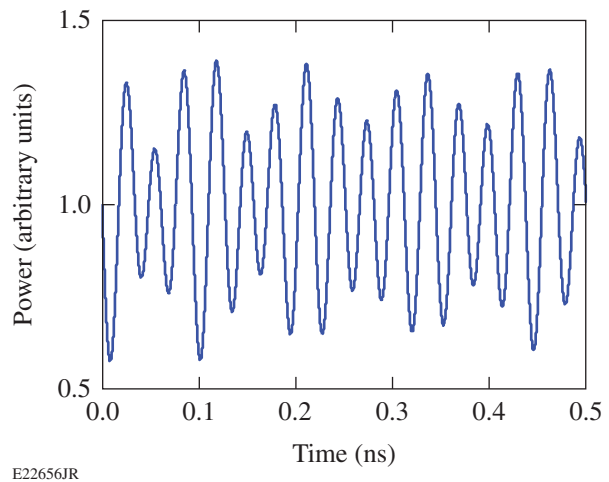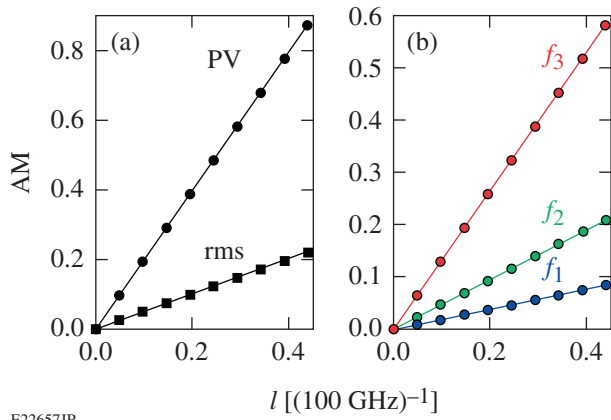
E22656JR

Figure 136.22
Temporal power after linear spectral amplitude modulation corresponding to $l = 0.44/(100\ \mathrm{GHz})$.

E22657JR

Figure 136.23
(a) Peak-to-valley and rms amplitude modulation (AM) versus magnitude of the linear spectral amplitude modulation. (b) Peak-to-valley AM at the frequencies f_j versus magnitude of the linear spectral amplitude modulation. The lines correspond to the simulations and the markers correspond to the analytical derivation.

2. Quadratic Spectral Phase

A quadratic spectral phase is the dominant phase term due to the chromatic dispersion of materials, e.g., laser glass and optical fibers, as well as the dominant term when propagating in a grating compressor. This impairment is represented in the spectral domain by the transfer function

$$\tau(\omega) = \exp\left(i\varphi_2\,\omega^2/2\right) \approx 1 + i\,\varphi_2\,\omega^2/2, \tag{20}$$

which leads to the temporal field

$$E' = E - i\,\frac{\varphi_2}{2}\,\frac{\partial^2 E}{\partial t^2}. \tag{21}$$

With the expression of the initial field given by Eq. (1), the resulting field is

$$E'(t) = E(t)\left\{1 - \frac{\varphi_2}{2}\sum_j m_j\,\Omega_j^2\cos\left(\Omega_j t\right)\right.$$

$$\left. + i\,\frac{\varphi_2}{2}\left[\sum_j m_j\,\Omega_j\sin\left(\Omega_j t\right)\right]^2\right\}. \tag{22}$$

When calculating the power (i.e., the modulus squared of the field), the imaginary component in Eq. (22) leads to a second-order term in φ_2. The power is given at first order by

$$P'(t) = 1 - \varphi_2\sum_j m_j\,\Omega_j^2\cos\left(\Omega_j t\right). \tag{23}$$

A quadratic spectral phase leads to amplitude modulation at the frequencies Ω_j with respective peak-to-valley amplitude

$$PV\left(\Omega_j\right) = 2\varphi_2 m_j\,\Omega_j^2. \tag{24}$$

Temporal modulations are observed at the modulation frequencies Ω_j, as for linear amplitude modulation, but the largest modulation corresponds to the frequency having the largest product $m_j\Omega_j^2$. An argument similar to that made about Eq. (16) shows that the overall peak-to-valley AM is

$$PV = 2\varphi_2\sum_j m_j\,\Omega_j^2, \tag{25}$$

while the rms AM is given by

$$rms = \varphi_2\sqrt{\sum_j m_j^2\,\Omega_j^4\big/2}. \tag{26}$$

Simulation results for quadratic spectral phase modulation are shown in Figs. 136.24 and 136.25. Figure 136.24 shows the modulated power after second-order dispersion $\varphi_2 = 1.01$ ps^2. Features similar to those of Fig. 136.22 are observed. Figure 136.25 shows the excellent agreement between the simulated and analytical results [Eqs. (25) and (26) for the peak-to-valley and rms AM, and Eq. (24) for the peak-to-valley AM at
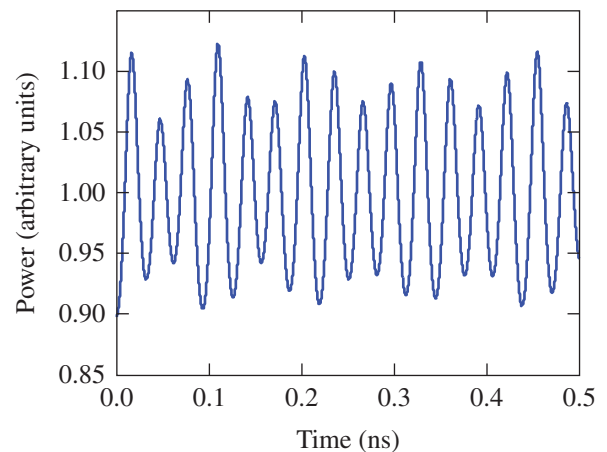
E22658JR

Figure 136.24
Temporal power after quadratic spectral phase corresponding to $\varphi_2 = 1.01$ ps^2.
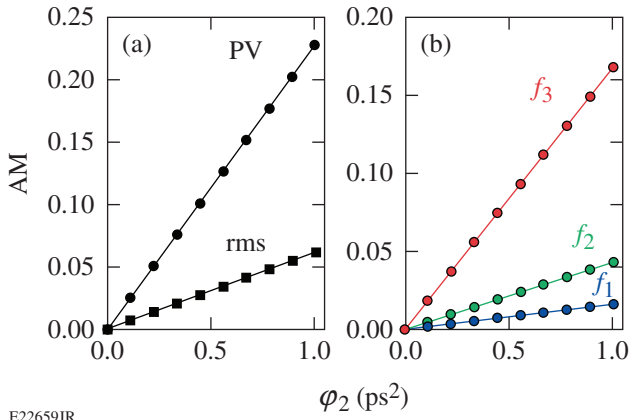
E22659JR

Figure 136.25
(a) Peak-to-valley and rms AM versus magnitude of the quadratic spectral phase modulation. (b) Peak-to-valley AM at the frequencies f_j versus magnitude of the quadratic spectral phase modulation. The lines correspond to the simulations and the markers correspond to the analytical derivation.

each frequency f_j] when the magnitude of the phase modulation is modified. The highest temporal modulation is observed at the frequency f_3 because that frequency corresponds to the largest quantity $m_j \Omega_j^2$, considering the parameters in Table 136.III.

3. Combination of Linear Spectral Amplitude and Quadratic Spectral Phase

Linear amplitude modulation and quadratic temporal phase modulation lead to temporal modulation at the frequencies Ω_j. Inspection of Eqs. (16) and (23) shows that the corresponding modulations occur in quadrature, each of them being either a sine or a cosine of the argument $\Omega_j t$. It is straightforward to show that the peak-to-valley AM at frequency Ω_j resulting from the in-quadrature modulations with respective PV amplitudes $2lm_j \Omega_j$ and $2\varphi_2 m_j \Omega_j^2$ is

$$\sqrt{\left(2\varphi_2 m_j \Omega_j^2\right)^2 + \left(2lm_j \Omega_j\right)^2},$$

i.e.,

$$PV\left(\Omega_j\right) = 2m_j \Omega_j \sqrt{\left(\varphi_2 \Omega_j\right)^2 + l^2}. \tag{27}$$

Since the modulation frequencies are not commensurate, there are times at which the extrema of the individual modulations are simultaneously reached, leading to the peak-to-valley AM

$$PV = 2 \sum_j m_j \Omega_j \sqrt{\left(\varphi_2 \Omega_j\right)^2 + l^2}. \tag{28}$$

The rms AM is obtained by considering that the resulting temporal power is the sum of uncorrelated sinusoidal functions oscillating at Ω_j with amplitude given by half the PV modulation expressed by Eq. (27). This leads to

$$rms = \sqrt{\sum_j m_j^2 \Omega_j^2 \left[\left(\varphi_2 \Omega_j\right)^2 + l^2\right] / 2}. \tag{29}$$

Figure 136.26 compares simulated and analytical results when the second-order dispersion is $\varphi_2 = 1.01$ ps^2 and the linear spectral amplitude modulation is modified. Excellent agreement is obtained, confirming the fact that Eqs. (27)–(29) accurately predict the influence of the combined phase and amplitude modulations. Similar agreement was observed when scanning the magnitude of the phase modulation for a given amplitude modulation.
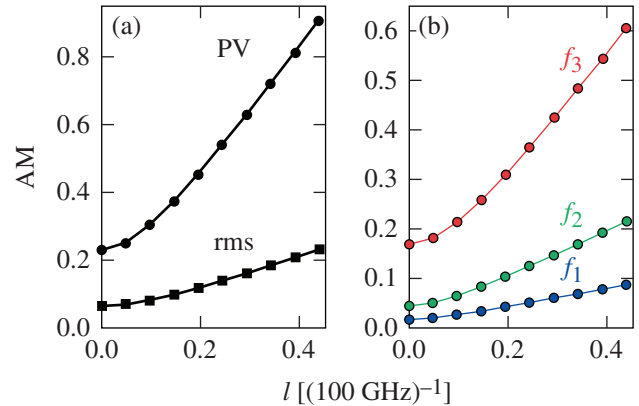
E22660JR

Figure 136.26
(a) Peak-to-valley and rms AM versus magnitude of the linear spectral amplitude for $\varphi_2 = 1.01$ ps^2. (b) Peak-to-valley AM at the frequencies f_j versus magnitude of the linear spectral amplitude for $\varphi_2 = 1.01$ ps^2. The lines correspond to the simulations and the markers correspond to the analytical derivation.

Impairments Leading to FM-to-AM Conversion at Intermodulation Frequencies
1. Quadratic Spectral Amplitude

Quadratic amplitude modulation occurs after propagation in a component at a frequency corresponding to an amplitude externum of the component's transfer function; for example, amplification at the peak of the gain of an amplifier. The corresponding transfer function is

$$\tau\left(\omega\right) = \sqrt{1 + q\omega^2} \approx 1 + \frac{q}{2}\omega^2, \tag{30}$$

leading to the temporal field

$$E' = E - \frac{q}{2} \frac{\partial^2 E}{\partial t^2}. \tag{31}$$

The resulting field is

$$E'(t) = E(t) \left\{ 1 + \frac{q}{2} \left[\sum_j m_j \Omega_j \sin \left(\Omega_j t \right) \right]^2 \right. $$

$$\left. + i \frac{q}{2} \sum_j m_j \Omega_j^2 \cos \left(\Omega_j t \right) \right\}, \tag{32}$$

where the real component proportional to q between the curled brackets will be the main modulation source since the complex quantity in the same brackets is squared when calculating the optical power. The resulting power, at first order in q, is

$$P'(t) = 1 + q \left[\sum_j m_j \Omega_j \sin \left(\Omega_j t \right) \right]^2. \tag{33}$$

When $q > 0$, the modulated power in Eq. (33) is higher than the average power of the signal in the absence of impairment at all times. This is explained by the fact that the transfer function [Eq. (30)] does not conserve the signal energy. Since one is interested in the temporal modulation of the power around its average value, and not around its value without impairment, AM determinations are scaled by the average power of the signal of Eq. (33),

$$1 + \frac{q}{2} \sum_j m_j^2 \Omega_j^2.$$

The minimum value of Eq. (33) is 1. The maximum value is obtained when all the modulations reach an extremum, and the resulting peak-to-valley AM is

$$PV = q \left(\sum_j m_j \Omega_j \right)^2 \Bigg/ \left(1 + \frac{q}{2} \sum_j m_j^2 \Omega_j^2 \right). \tag{34}$$

The rms AM on the resulting power is calculated from Eq. (33), leading to

$$\text{rms} = \frac{q \sqrt{\sum_j m_j^4 \Omega_j^4 \Big/ 8 + \sum_{j,k} m_j^2 m_k^2 \Omega_j^2 \Omega_k^2}}{\left(1 + \frac{q}{2} \sum_j m_j^2 \Omega_j^2 \right)}. \tag{35}$$

Equation (33) can be developed into a sum of terms proportional to $\sin(\Omega_j t) \sin(\Omega_k t)$. The choice of $j = k$ leads to a term oscillating at the frequency $2\Omega_j$ with PV amplitude $q m_j^2 \Omega_j^2$. The two terms corresponding to the choice (j,k) and (k,j) with $j \neq k$ lead to modulations at $\Omega_j + \Omega_k$ and $\Omega_j - \Omega_k$, each of them with a PV amplitude $2 q m_j m_k \Omega_j \Omega_k$. The resulting AM's at these frequencies are

$$PV \left(2\Omega_j \right) = q m_j^2 \Omega_j^2 \Bigg/ \left(1 + \frac{q}{2} \sum_j m_j^2 \Omega_j^2 \right) \tag{36}$$

and

$$PV \left(\Omega_j \pm \Omega_k \right) = 2 q m_j m_k \Omega_j \Omega_k \Bigg/ \left(1 + \frac{q}{2} \sum_j m_j^2 \Omega_j^2 \right). \tag{37}$$

The modulation amplitudes at the frequencies $\Omega_j + \Omega_k$ and $\Omega_j - \Omega_k$ are identical. Simulation and analytical results for quadratic spectral amplitude modulation are displayed in Figs. 136.27 and 136.28. Figure 136.27 shows the complex behavior of the amplitude modulation, in particular the clear presence of modulations at multiple frequencies. Figure 136.28
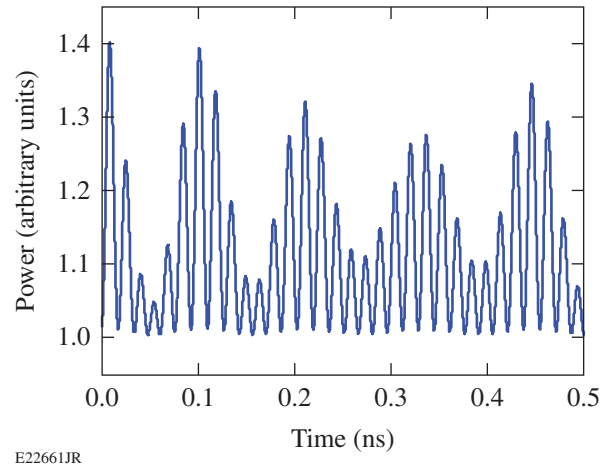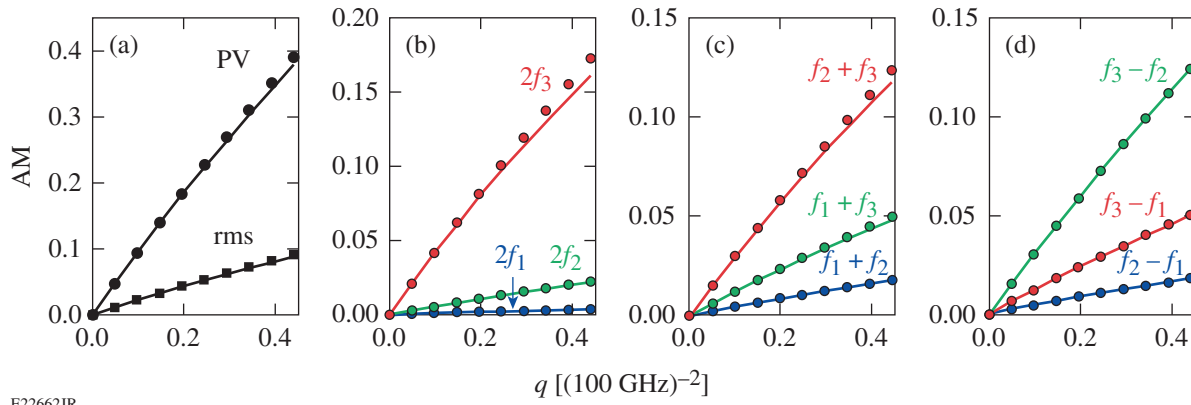

E22661JR

Figure 136.27
Temporal power after quadratic spectral amplitude modulation corresponding to $q = 0.44/(100 \text{ GHz})^2$.

E22662JR

Figure 136.28
(a) Peak-to-valley and rms AM versus magnitude of the quadratic spectral amplitude modulation. [(b)–(d)] Peak-to-valley AM at the frequencies $2f_j$, $f_j + f_k$, and $f_j - f_k$ versus magnitude of the quadratic spectral amplitude modulation. The lines correspond to the simulations and the markers correspond to the analytical derivation.

details the PV and rms AM for the temporal power as well as the frequency-resolved peak-to-valley AM. The simulation results are in excellent agreement with the analytical results from Eqs. (34)–(37). The highest modulations are observed at the frequencies $2f_3$, $f_2 + f_3$, and $f_3 - f_2$, which contribute most of the PV modulation observed in the time domain. The first two of these frequencies are larger than 50 GHz, while the third is approximately 10 GHz. Bandwidth limitation in a temporal diagnostic might hinder the ability to accurately characterize the temporal modulation. Detection of a modulation at a low frequency (e.g., $\Omega_j - \Omega_k$) indicates the presence of modulation at a higher frequency (e.g., $\Omega_j + \Omega_k$) with identical amplitude.

2. Cubic Spectral Phase

A cubic spectral phase is typically the leading phase impairment once the quadratic spectral phase has been compensated over the bandwidth of the source. Because the relative signs of the second-order and third-order dispersions for propagation in materials and in a grating compressor are different, a cubic spectral phase is induced when a grating compressor is used to compensate the chromatic dispersion of optical fibers. The transfer function is represented by

$$\tau\left(\omega\right) = \exp\left(i\varphi_3\omega^3/6\right) \approx 1 + i\varphi_3\omega^3/6. \quad (38)$$

This leads to the output temporal field

$$E' = E + \frac{\varphi_3}{6}\frac{\partial^3 E}{\partial t^3}. \quad (39)$$

The expression for the third-order derivative of Eq. (1) is lengthy, but only the real terms should be kept since they are the ones leading to an approximation of the modulated power at first order in φ_3 when inserted into Eq. (39). The modulated power is given by

$$P'(t) = 1 - \varphi_3 \sum_j m_j \Omega_j \sin\left(\Omega_j t\right) \sum_j m_j \Omega_j^2 \cos\left(\Omega_j t\right). \quad (40)$$

For this impairment, the spectrally resolved amplitude modulation is calculated first. The product of the two summation terms in Eq. (40) gives modulations at the frequencies $2\Omega_j$ and at the intermodulation frequencies $\Omega_j \pm \Omega_k$. The term at $2\Omega_j$ corresponds to

$$\varphi_3 m_j \Omega_j \sin\left(\Omega_j t\right) m_j \Omega_j^2 \cos\left(\Omega_j t\right) =$$
$$\varphi_3 m_j^2 \Omega_j^3 \sin\left(2\Omega_j t\right)/2. \quad (41)$$

The peak-to-valley AM at $2\Omega_j$ is

$$\text{PV}\left(2\Omega_j\right) = \varphi_3 m_j^2 \Omega_j^3. \quad (42)$$

The terms corresponding to $j \neq k$ are

$$\varphi_3 m_j m_k \Omega_j \Omega_k \left[\Omega_k \sin\left(\Omega_j t\right)\cos\left(\Omega_k t\right)\right.$$
$$\left. + \Omega_j \sin\left(\Omega_k t\right)\cos\left(\Omega_j t\right)\right], \quad (43)$$

which can be expressed using a trigonometric identity for the product of a sine and cosine as

$$\varphi_3 m_j m_k \Omega_j \Omega_k \left\{ (\Omega_j + \Omega_k) \sin \left[(\Omega_j + \Omega_k) t \right] \right.$$
$$\left. + (\Omega_k - \Omega_j) \sin \left[(\Omega_j - \Omega_k) \right] \right\} \bigg/ 2. \qquad (44)$$

The peak-to-valley AM for these sum/difference frequencies is therefore

$$PV(\Omega_j \pm \Omega_k) = \varphi_3 m_j m_k \Omega_j \Omega_k (\Omega_j \pm \Omega_k), \qquad (45)$$

where it has been assumed that $\Omega_j > \Omega_k$.

The rms AM is obtained by noting that the average temporal value of Eq. (40) is equal to 1 because the spectral field is phase modulated but not amplitude modulated. One can then write

$$rms^2 = \varphi_3^2 \int \left[\sum_j m_j \Omega_j \sin(\Omega_j t) \right]^2$$
$$\times \left[\sum_j m_j \Omega_j^2 \cos(\Omega_j t) \right]^2 dt. \qquad (46)$$

Each square in the previous equation can be developed, and considering that the integral of a product of sinusoidal functions with noncommensurate frequencies is zero if it contains odd powers of a sinusoidal function (either sine or cosine) at a particular frequency, Eq. (46) can be rewritten as

$$rms^2 = \varphi_3^2 \int \sum_j m_j^2 \Omega_j^2 \sin^2(\Omega_j t) \sum_j m_j^2 \Omega_j^4 \cos^2(\Omega_j t) dt \quad (47)$$

and as

$$rms^2 = \varphi_3^2 \int \left[\sum_j m_j^4 \Omega_j^6 \sin^2(\Omega_j t) \cos^2(\Omega_j t) \right.$$
$$\left. + \sum_{j \neq k} m_j^2 m_k^2 \Omega_j^2 \Omega_k^4 \sin^2(\Omega_j t) \cos^2(\Omega_k t) \right] dt. \qquad (48)$$

Equation (48) can be calculated to obtain the rms AM in the presence of third-order dispersion,

$$rms = \frac{\varphi_3}{2} \sqrt{ \sum_j m_j^4 \Omega_j^6 \big/ 2 + \sum_{j \neq k} m_j^2 m_k^2 \Omega_j^2 \Omega_k^4 }. \qquad (49)$$

The peak-to-valley AM is difficult to obtain in the general case because the different sinusoidal components in Eq. (40) have different frequencies and reach their maxima at different times, but a minimal and maximal bound for that quantity can be obtained. A minimal bound PV_{min} is obtained by considering that the peak-to-valley modulation must be larger than the modulation amplitude obtained considering any two different temporal arguments in Eq. (40). One can consider a time value for which each sine and cosine in that equation is equal to $\pm 1 \big/ \sqrt{2}$, leading to the inequality

$$PV \geq PV_{min} = \varphi_3 \sum_j m_j \Omega_j \sum_j m_j \Omega_j^2. \qquad (50)$$

A maximal bound PV_{max} is obtained by considering that, at this approximation order, only the modulations at all the frequencies $2\Omega_j$ and $\Omega_j + \Omega_k$ contribute to the temporal modulation. The resulting peak-to-valley AM is smaller than the sum of individual peak-to-valley AM (the equality is reached only if a time exists when all the individual modulations reach their maximum and another time when they all reach their minimum). The maximal bound is the sum of Eqs. (42) and (45), leading to the inequality

$$PV \leq PV_{max} = PV_{min} + \varphi_3 \sum_{j > k} m_j m_k \Omega_j \Omega_k (\Omega_j - \Omega_k). \qquad (51)$$

The span of the interval $PV_{max} - PV_{min}$ is small compared to the predicted range of peak-to-valley modulation values since the summation in Eq. (51) contains terms that are small, because either some of the modulation indices are small or the frequency differences are smaller than the frequency sums. In particular, one has $PV_{min} = PV_{max} = \varphi_3 m_1^2 \Omega_1^3$ for a single modulation frequency.

Figures 136.29 and 136.30 display results pertaining to temporal AM in the presence of a cubic spectral phase. The existence of multiple modulation frequencies is clearly visible in Fig. 136.29. Figure 136.30(a) shows the analytical and simulation results for the peak-to-valley and rms modulation on the test signal as a function of the cubic spectral modulation magnitude. Excellent agreement is obtained for the rms AM. The peak-to-valley AM obtained by simulation is correctly bracketed by the AM calculated with Eqs. (50) and (51). The frequency-resolved peak-to-valley AM reveals that the AM is dominated by contributions at the frequencies $2f_3$ and $f_2 + f_3$. Contrary to the case of quadratic gain modulation, AM at
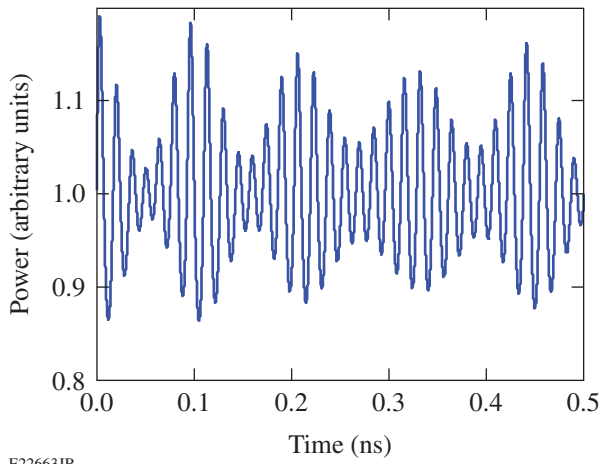
E22663JR

Figure 136.29
Temporal power after cubic spectral phase modulation corresponding to $\varphi_3 = 4.8$ ps^3.
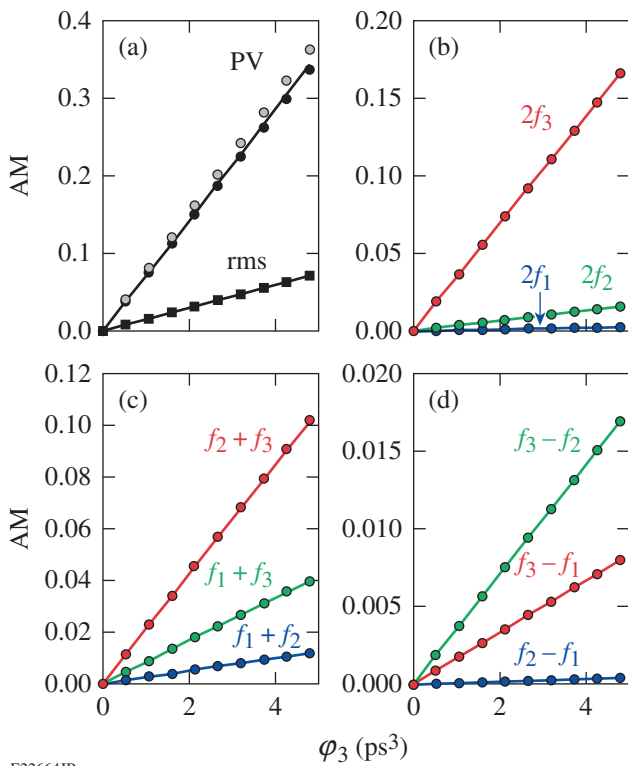

E22664JR

Figure 136.30
(a) Peak-to-valley and rms AM versus magnitude of the cubic spectral phase modulation. The lower and higher bounds for the peak-to-valley AM are shown with black and gray markers, respectively. [(b)–(d)] Peak-to-valley AM at the frequencies $2f_j$, $f_j + f_k$, and $f_j - f_k$ versus magnitude of the cubic spectral phase modulation. The lines correspond to the simulations and the markers correspond to the analytical derivation.

the low frequency $f_3 - f_2$ is much smaller than the AM at $f_2 + f_3$. A signal impaired by third-order dispersion detected by a low-bandwidth temporal diagnostic might seem of much better quality than it actually is.

Additional Considerations

At first order in the modulation resulting from each impairment, the power of an impaired signal is

$$P'(t) = 1 + l \sum_j m_j \Omega_j \sin(\Omega_j t) - \varphi_2 \sum_j m_j \Omega_j^2 \cos(\Omega_j t)$$

$$+ q \left[\sum_j m_j \Omega_j \sin(\Omega_j t) \right]^2 - \varphi_3 \sum_j m_j \Omega_j \sin(\Omega_j t)$$

$$\times \sum_j m_j \Omega_j^2 \cos(\Omega_j t), \qquad (52)$$

where the summations correspond to linear amplitude modulation, quadratic phase modulation, quadratic amplitude modulation, and cubic phase modulation. Because the Fourier transform is a linear operator, the frequency signature of the modulated power can partially reveal the origin of the impairments: temporal modulations at some of the phase-modulation frequencies indicate that the signal is impaired by a linear amplitude modulation or quadratic phase modulation, while temporal modulations at some of the sum or difference frequencies indicate that the signal is impaired by a quadratic amplitude modulation or cubic phase modulation.

The ratio of the AM at different frequencies can be used in some cases to identify the source of impairment. For example, this ratio for frequencies f_j and f_k is $m_j f_j / m_k f_k$ when the main impairment is linear amplitude modulation [Eq. (17)] and $m_j f_j^2 / m_k f_k^2$ when the main impairment is quadratic phase modulation [Eq. (24)]. Since the modulation indices and frequencies are known, such quantitative analysis can reveal the origin of the temporal modulation. When these two impairments are present, a more-precise study of the ratio of the AM at different frequencies is likely to reveal their respective contributions—Eq. (27) contains only two unknowns: the coefficient for linear amplitude modulation l and the coefficient for quadratic phase modulation φ_2. These unknowns can be determined if at least two modulation frequencies are present in the signal. With more than two frequencies, the best set of coefficients can be determined in the least-squares sense. Similar considerations can be applied to modulations observed

234

at intermodulation frequencies when quadratic amplitude modulation and cubic phase modulation are present.

Analytical expressions for the amplitude modulation resulting from impairments of a phase-modulated signal are the necessary starting points for understanding the requirements of temporal diagnostics used to characterize the resulting signals. In practical situations, a diagnostic with a flat response up to a frequency as high as twice the highest phase-modulation frequency in the system is necessary and sufficient to capture the time-domain signal, provided that the impairments are limited to those treated in this article. Insufficient bandwidth leads to an underestimate of the amplitude modulation present on the signal. For signals corresponding to the parameters in Table 136.III, intermodulation frequencies can be at frequencies difficult to reach with the current state-of-the-art single-shot oscilloscopes and photodetector (e.g., $2f_3 \sim 64$ GHz). In general, AM is also generated at lower frequencies (e.g, $f_3 - f_2 \sim 10$ GHz), but a photodetection system with insufficient bandwidth might lead to a significant underestimate of the physical modulation, particularly in the presence of cubic phase.

Conclusions

The spectral and temporal properties of optical signals generated by multiple sinusoidal phase modulations of a monochromatic source have been studied. A formalism for the statistical prediction of the optical spectrum of these signals has been developed based on the central limit theorem, showing the convergence of the spectrum of a signal with multiple phase modulations to a Gaussian spectrum with identical rms bandwidth, which can be calculated analytically from the modulation parameters, and the associated convergence of their cumulative density functions. The comparison between the directly simulated spectrum and predicted Gaussian spectrum for a finite number of frequencies confirmed the asymptotic result and showed that in most conditions, the frequency interval containing 98% of the energy can be predicted from the modulation parameters, although there is significant variation when the number of frequencies is low. FM-to-AM conversion on signals with multiple phase modulations has been analytically described for typical spectral impairments to extend the results known for signals modulated at a single frequency. An excellent agreement with direct simulations has been observed. These results are useful in understanding the current limitations of the laser systems using phase modulation along with the associated subsystems and diagnostics, and in optimizing the engineering of existing and future systems.

REFERENCES

1. J. D. Lindl *et al*., Phys. Plasmas **11**, 339 (2004).

2. R. L. McCrory, D. D. Meyerhofer, R. Betti, R. S. Craxton, J. A. Delettrez, D. H. Edgell, V. Yu Glebov, V. N. Goncharov, D. R. Harding, D. W. Jacobs-Perkins, J. P. Knauer, F. J. Marshall, P. W. McKenty, P. B. Radha, S. P. Regan, T. C. Sangster, W. Seka, R. W. Short, S. Skupsky, V. A. Smalyuk, J. M. Soures, C. Stoeckl, B. Yaakobi, D. Shvarts, J. A. Frenje, C. K. Li, R. D. Petrasso, and F. H. Séguin, Phys. Plasmas **15**, 055503 (2008).

3. C. A. Haynam *et al*., Appl. Opt. **46**, 3276 (2007).

4. N. Fleurot, C. Cavailler, and J. L. Bourgade, Fusion Eng. Des. **74**, 147 (2005).

5. J. R. Murray *et al*., J. Opt. Soc. Am. B **6**, 2402 (1989).

6. P. J. Wisoff *et al*., in *Optical Engineering at the Lawrence Livermore National Laboratory II: The National Ignition Facility*, edited by M. A. Lane and C. R. Wuest (SPIE, Bellingham, WA, 2004), Vol. 5341, pp. 146–155.

7. S. Hocquet *et al*., Appl. Opt. **47**, 3338 (2008).

8. J. D. Kilkenny, S. G. Glendinning, S. W. Haan, B. A. Hammel, J. D. Lindl, D. Munro, B. A. Remington, S. V. Weber, J. P. Knauer, and C. P. Verdon, Phys. Plasmas **1**, 1379 (1994).

9. S. Skupsky, R. W. Short, T. Kessler, R. S. Craxton, S. Letzring, and J. M. Soures, J. Appl. Phys. **66**, 3456 (1989).

10. J. E. Rothenberg, J. Opt. Soc. Am. B **14**, 1664 (1997).

11. *LLE Review Quarterly Report* **114**, 73, Laboratory for Laser Energetics, University of Rochester, Rochester, NY, LLE Document No. DOE/NA/28302-826, OSTI ID 935224 (2008).

12. Y. Lin, T. J. Kessler, and G. N. Lawrence, Opt. Lett. **20**, 764 (1995).

13. T. J. B. Collins, J. A. Marozas, K. S. Anderson, R. Betti, R. S. Craxton, J. A. Delettrez, V. N. Goncharov, D. R. Harding, F. J. Marshall, R. L. McCrory, D. D. Meyerhofer, P. W. McKenty, P. B. Radha, A. Shvydky, S. Skupsky, and J. D. Zuegel, Phys. Plasmas **19**, 056308 (2012).

14. J. H. Kelly, A. Shvydky, J. A. Marozas, M. J. Guardalben, B. E. Kruschwitz, L. J. Waxer, C. Dorrer, E. Hill, A. V. Okishev, and J.-M. Di Nicola, in *High Power Lasers for Fusion Research II*, edited by A. A. S. Awwal (SPIE, Bellingham, WA, 2013), Vol. 8602, Paper 86020D.

15. B. E. Kruschwitz, J. H. Kelly, C. Dorrer, A. V. Okishev, L. J. Waxer, G. Balonek, I. A. Begishev, W. Bittle, A. Consentino, R. Cuffney,

E. Hill, J. A. Marozas, M. Moore, R. G. Roides, and J. D. Zuegel, in *High Power Lasers for Fusion Research II*, edited by A. A. S. Awwal (SPIE, Bellingham, WA, 2013), Vol. 8602, Paper 86020E.

16. C. Dorrer, R. Roides, R. Cuffney, A. V. Okishev, W. A. Bittle, G. Balonek, A. Consentino, E. Hill, and J. D. Zuegel, IEEE J. Sel. Top. Quantum Electron. **19**, 3500112 (2013).

17. J. E. Rothenberg, D. F. Browning, and R. B. Wilcox, in *Third International Conference on Solid State Lasers for Application to Inertial Confinement Fusion*, edited by W. H. Lowdermilk (SPIE, Bellingham, WA, 1999), Vol. 3492, pp. 51–61.

18. H. Cao *et al.*, Appl. Opt. **50**, 3609 (2011).

19. S. Hocquet, G. Lacroix, and D. Penninckx, Appl. Opt. **48**, 2515 (2009).

20. L. W. Couch III, *Digital and Analog Communication Systems*, 3rd ed. (Macmillan Publishing Company, New York, 1990).

21. S. Vidal, J. Luce, and D. Penninckx, Opt. Lett. **36**, 3494 (2011).

22. D. Penninckx *et al.*, J. Lightwave Technol. **24**, 4197 (2006).

23. S. Hocquet *et al.*, Appl. Opt. **49**, 1104 (2010).

24. J. W. Goodman, *Statistical Optics* (Wiley, New York, 2000).

25. D. Collett, *Modelling Binary Data*, 2nd ed. (Chapman & Hall/CRC, Boca Raton, FL, 2003).